GPU-based simulation of echocardiography volumes using quantitative fiber-angle-to-backscatter measurements

Yociss, Megan, Fei, Baowei

Megan Yociss, Baowei Fei, "GPU-based simulation of echocardiography volumes using quantitative fiber-angle-to-backscatter measurements," Proc. SPIE 11602, Medical Imaging 2021: Ultrasonic Imaging and Tomography, 116020U (24 February 2021); doi: 10.1117/12.2581962

SPIE.

Event: SPIE Medical Imaging, 2021, Online Only

GPU-Based Simulation of Echocardiography Volumes Using Quantitative Fiber-Angle-to-Backscatter Measurements

Megan Yociss [a], Baowei Fei *[a,b]

[a]The University of Texas at Dallas, Department of Bioengineering, Richardson, TX
[b]The University of Texas Southwestern Medical Center, Department of Radiology, Dallas, TX

*E-mail: bfei@utdallas.edu, Website: https://fei-lab.org

ABSTRACT

The intensity of backscattered ultrasound signal from heart muscle is known to be related to the angle between cardiac fibers and the insonification direction. In this work, a GPU-based method of simulating three-dimensional (3D) echocardiographic images from an empirically derived angle-to-backscatter relationship is developed and validated. Images of a rotating fiber phantom are simulated, and it is validated that the angle-to-backscatter relationship is accurately reflected by the simulated envelope data. In a second experiment, echocardiography images are simulated from a diffusion tensor magnetic resonance imaging (DT-MRI) volume of a canine heart to demonstrate that the method produces view-dependent speckle. 3D volumes of a parametrically generated ideal left ventricle phantom are also simulated and processed into fiber orientation maps using the underlying quantitative parameters. Images are simulated based on the characteristics of a 35-by-32 two-dimensional (2D) matrix array probe and a clinical one-dimensional (1D) phased array probe. The processed fiber volumes exhibit good agreement with the virtual phantom's ground truth, having an average acute angle error (AAE) of less than 10 degrees for both probes. The simulation method is fast and opens a new approach for ultrasound fiber imaging.

Keywords: Echocardiography, cardiac fiber orientation, myocardia, quantification, backscatter, GPU, volumetric ultrasound imaging, ultrasound simulation, matrix array, ultrasound probe

1. INTRODUCTION

Accurate estimation of cardiac fiber orientations is an important problem since changes in fiber architecture can be an early indicator of heart disease[1]. Although diffusion tensor magnetic resonance imaging (DT-MRI) has been explored to visualize cardiac fibers primarily in two-dimensional (2D) studies, three dimensions (3D) *in vivo* cardiac DT-MRI is challenging because of cardiac and respiration motion. Additionally, DT-MRI with gating can be time-consuming and expensive. Ultrasound imaging is therefore regarded as a possible alternative. A few approaches have been explored for fiber quantification using ultrasound. Ultrasound backscatter tensor imaging[2] uses the spatial coherence of backscattered waves to estimate fiber orientations within the plane perpendicular to the beam. Another approach is the deformation of co-registered T1 and DT-MRI volumes to 3D ultrasound volumes[3]. In a third approach[4], the empirically derived dependence of image pixel intensities on fiber orientations was used to create maps of fiber angles relative to the imaging plane. 3D orientation volumes were created by mechanically rotating a clinical phased array probe around excised sheep hearts in small angle increments.

The use of 2D matrix array probes for echocardiography has been explored in several recent studies. Unlike conventional phased array probes, which can only acquire images within a single plane, matrix array probes are capable of acquiring 3D volumes of data. Additionally, very high frame rates can be achieved by transmitting fully diverging spherical waves and focusing only in reception. However, there are still many barriers to the widespread clinical use of matrix array probes for volumetric quantitative heart imaging, such as limited spatiotemporal resolution and the requirement of multiple synchronized scanning systems to drive the elements of a typical 35-by-32 probe for good image quality. It was determined that an optimal sparse selection of elements matrix array elements, connected to a single scanning system, could be used for 3D planar echocardiography imaging in real time[5]. A fiber quantification method was

Medical Imaging 2021: Ultrasonic Imaging and Tomography, edited by Brett C. Byram, Nicole V. Ruiter, Proc. of SPIE Vol. 11602, 116020U · © 2021 SPIE
CCC code: 1605-7422/21/$21 · doi: 10.1117/12.2581962

previously reported,[4] which relies on rotated planar images obtained with a rotating 1D phased array probe. In this study, we aim to demonstrate via simulations that similar results can be achieved using a sparsely wired matrix array without the requirement of mechanical rotation.

Ultrasound fiber orientation imaging methods are known to be difficult to validate by comparison with DT-MRI, often due to registration errors[4]. Therefore, we aim to develop a simulation method incorporating ground truth orientation information that yields an inherently co-registered volume for quantification. A number of methods for ultrasound simulation have previously been developed, including Field II[6], COLE[7], and optical ray tracing[8]. However, standard implementations of these methods do not include the effects of tissue anisotropy on scattering, which is necessary for the simulation of biologically realistic images of the heart. Real echocardiography images were previously used to generate a set of scatterers with varying amplitudes based on their location in the myocardium.[9] The scatterers were then used for forward simulation with COLE, yielding realistic images for several different probe models. However, the insonification direction was not considered in the calculation of scatterer amplitudes, so this method is not suitable for simulating view-dependent speckle. In another study[10], view-dependent ultrasound images of rat hearts were simulated using a two-step process. As a preprocessing step, randomly generated scatterer grids were smoothed using directional filtering with kernels derived from DT-MRI volumes. The resulting scatterer grids were used as input to the Fast Ultrasound Simulation in K-space method (FUSK)[11]. This method was shown to produce view-dependent speckle having good agreement with real ultrasound images, but it requires a computationally expensive preprocessing step and does not include a quantitative relationship between backscatter intensity and insonification direction. In this work, we extend the fast COLE algorithm to include a quantitative angle-to-backscatter relationship, and demonstrate that it is suitable for validating angle-backscatter fiber orientation imaging.

2. METHODS

2.1 Anisotropic Angle-to-Backscatter Relationship

The backscattered intensity from cardiac fibers is known to be at a minimum when the fibers are parallel to the insonification direction, and at a maximum when they are perpendicular to the insonification direction. An angle-to-backscatter relationship was previously reported for rat myocardium derived from empirical data[12]. Cylindrical cores of excised tissue were imaged at 5-degree rotations using a 21 MHz transducer attached to a VisualSonics Vevo 2100 small animal ultrasound system (FujiFilm VisualSonics, Toronto, ON). The mean data for each angle were then fit with a function of even powers of sines and cosines, which was given as:

$$I(\theta) = C_1 + C_2 \cdot \sin^6\theta + C_3 \cdot \cos^6\theta \quad (1)$$

where $I(\theta)$ is the intensity of the signal measured in decibels (dB) within the cylindrical phantom at rotation angle θ relative to the transducer, and C_n are constants. The constants were reported as C_2=14.2 and C_3=-7.1. We used this function in all simulations to calculate the amplitude of scatterers relative to the beam direction, but any organism-specific relationship could be used. We set C_1 to -14.2 so that I(90 degrees) = 0 dB, which corresponds to a backscatter intensity of 100%.

2.2 Point Spread Function (PSF) Modeling

We used Field II to precompute the spatially varying lateral and elevational profiles of the ultrasound system PSF for use in simulations[13]. We simulated images based on a 35-by-32 element, 3 MHz matrix array probe that is frequently used in echocardiography research (Vermon S.A., Tours, France) with an optimal distribution of controlled elements[5] (Figure 1). The elements are selected from the matrix according to a density-tapered Fermat's spiral pattern with 256 seeds. This element configuration reduces grating and side lobe artifacts, and can be driven by a single 256-channel scanner, making it more practical for clinical use than a fully connected probe requiring multiple synchronized scanners. We also simulated images based on the characteristics of a 3 MHz, 1D phased array probe (GE Healthcare, Waukesha, WI) that is used in clinical imaging.

We computed 3D profiles for the lateral and elevational PSF components orthogonal to the scanline direction to simulate two different approaches for volume acquisition. For the first approach, the 2D matrix array is used to insonify the entire

plane of interest with a single transmission event. The beam is transmitted from a virtual source behind the transducer at (0, 0, -9) mm and is focused in the y-z plane at 50 mm, creating a planar beam that diverges in the x-z plane (Figure 2A, 2B). Delays for the array elements were calculated[14]. Electronic focusing is performed in reception (Figure 2C). Consecutive rotated single plane transmissions with steered focusing in reception can be used to image several planes of interest at a very high frame rate, making this approach feasible for *in vivo* cardiac imaging. For the second sequence, the 1D phased array probe is used to transmit a beam with a physical focus at a radial distance of 80 mm, and dynamic focusing is used in reception (Figure 2D). A series of steered single line transmissions can be used to image the plane parallel to the face of the probe. The probe can be mechanically rotated to image multiple planes of interest to obtain a 3D volume. We modeled the axial component of the PSFs as a Gaussian-modulated sinusoidal radiofrequency (RF) pulse for both probes[13].

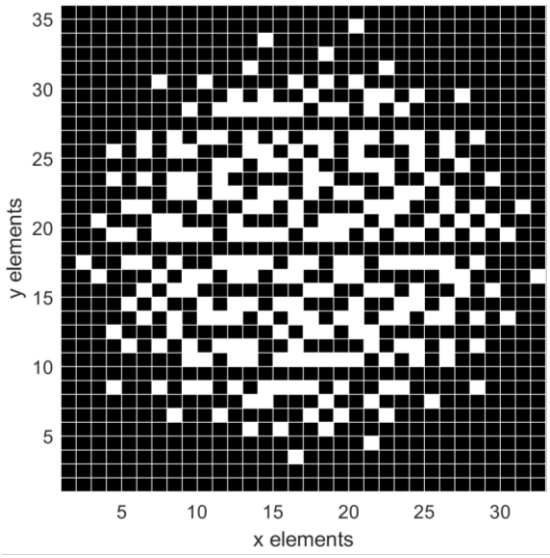

Figure 1. Active elements selected from a 2D matrix array probe according to a density-tapered spiral pattern.

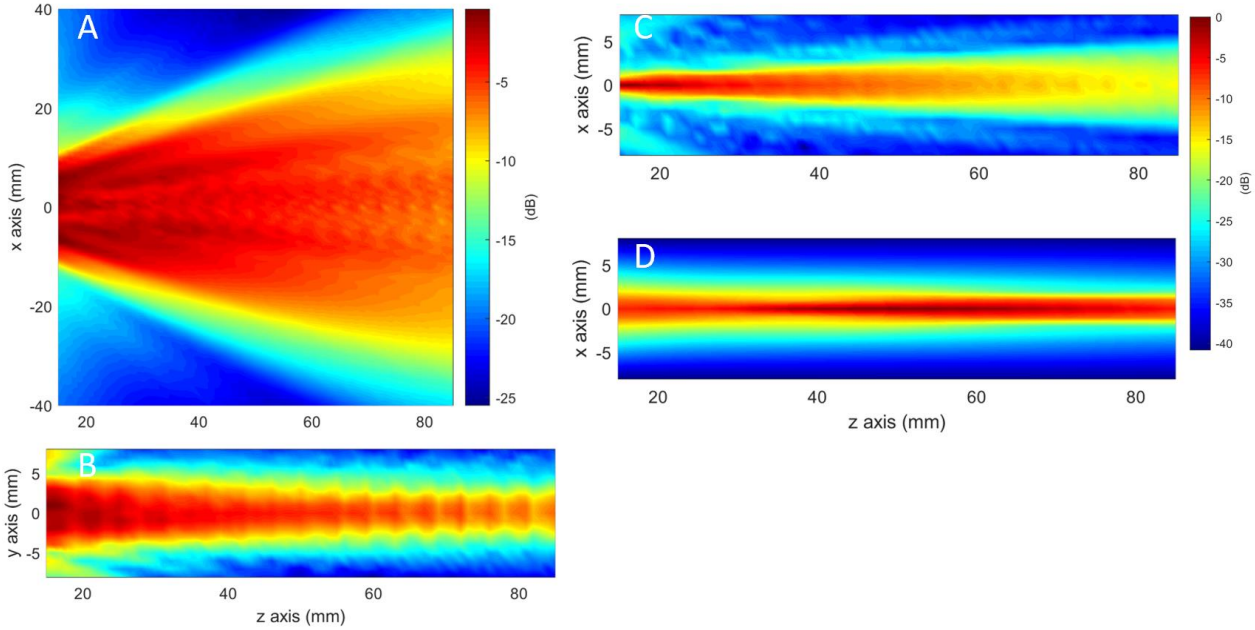

Figure 2. Ultrasound field emitted by a 2D matrix array transmitting a beam that diverges in the x-z plane (A) and is focused in the y-z plane (B); lateral PSF profile for the planar diverging beam transmission with electronic focusing in reception (C); lateral PSF profile for a focused beam generated by a 1D phased array probe (D).

2.3 Image Simulation on the GPU Using Anisotropic COLE and Fiber Image Processing

For fast image simulations, we implemented an extended version of the COLE algorithm. Our implementation is written in Python and accelerated using the Numba library for compiling functions to run on CUDA-enabled GPUs[15]. As in standard implementations of COLE[7,13], an RF image of size (scanlines, RF samples) is computed from a collection of scatterers distributed in 3D space with randomly assigned amplitudes. Scatterers are first projected onto each scanline according to their amplitude and location within the supplied profile of the lateral and elevational PSF as represented by cylindrical coordinates (θ, r, y). Then, each individual scanline is convolved with the axial component of the PSF. In our implementation, we added an additional step to modify a scatterer's amplitude according to the dot product of a unit vector representing its orientation and the direction vector of the ultrasound beam, and the underlying angle-to-backscatter relationship. The summed projection of scatterers is calculated separately on the GPU for each individual RF pixel. The projection algorithm for a single RF pixel, the location of which is given in polar coordinates based on its scanline and sample index, is described by the following simplified pseudocode:

Algorithm 1 (Anisotropic COLE):

Inputs: Scatterers (position(x, z, y, r), orientation(x, z, y), amplitude), PSF_profile(θ, r, y), RF_pixel(θ, r), Angle_backscatter = Equation 1

Output: RF_pixel_amplitude

```
beam_direction = ( sin( RF_pixel(θ) ), cos( RF_pixel(θ) ), 0 )
RF_pixel_amplitude = 0.0
for scatterer in scatterers where scatterer.position(r) = RF_pixel.r:
        position_θ = arctan( scatterer.position(x) / scatterer.position(z) )
        scatterer_amplitude = scatterer.amplitude * PSF_profile( position_θ, scatterer.position(r), scatterer.position(y) )
        if scatterer.orientation:
                fiber_θ = arccos( dot_product( beam_direction, scatterer.orientation ) )
                fiber_backscatter = Angle_backscatter( fiber_θ )
                scatterer_amplitude = scatterer_amplitude * fiber_backscatter
        RF_pixel_amplitude = RF_pixel_amplitude + scatterer_amplitude
return RF_pixel_amplitude
```

A set of rotated images, representing either mechanical rotation for the phased array probe or electronic rotation for the matrix probe, can be obtained by rotating the scatterer volume around the probe's central axis. After RF images are simulated, they can be post-processed into brightness mode (B-mode) images using envelope detection, log compression, and scan conversion algorithms similar to the ones performed by real ultrasound systems. If images for multiple rotated planes have been simulated, they can be used to interpolate a 3D volume.

Since the goal of this research was to develop a simulation method that can be used for fiber quantification method validation, we implemented an additional image processing step similar to the method reported[4] for constructing fiber images and volumes. After the envelope signal of size (scanlines, RF samples) is simulated, a 2 mm averaging window is applied to each scanline, and a five-point binomial filter is applied at each RF sample index. The filtered image is then converted from polar coordinates to Cartesian coordinates with bilinear interpolation. Each row is converted to dB using its maximum value, which is assumed to represent a pixel where fibers are perfectly perpendicular to the beam direction. Equation 1 and the given coefficients are then used to determine the fiber direction relative to the ultrasound beam in each pixel. The filtering, scan conversion, and 3D interpolation steps were accelerated with Numba for fast fiber volume formation.

2.4 Parametric Fiber Phantom Imaging

In order to determine if our algorithm produces images that accurately reflect the underlying angle-to-backscatter relationship, we simulated images of simple, parametrically defined cylindrical fiber phantoms. The image field of view was first divided into five equal sectors, and the beam direction of each sector's central scanline was calculated. Then, scatterers were distributed in each sector within a cylindrical phantom located on the central scanline at an axial depth of 60 mm, and having a radius of 3 mm and a height of 5 mm. Each scatterer's orientation was set as the rotation of the sector's central beam direction in the x-z plane by the sector number multiplied by 22.5 degrees (Figure 3). Therefore, the phantoms were set to represent cardiac tissue cores with fiber orientations from 0 degrees to 90 degrees in 22.5-

degree increments. The scatterer density was set to 500 per cubic mm, which is sufficient for fully developed speckle. RF images were simulated of the fiber phantoms, and the signal envelope was obtained using the Hilbert transform.

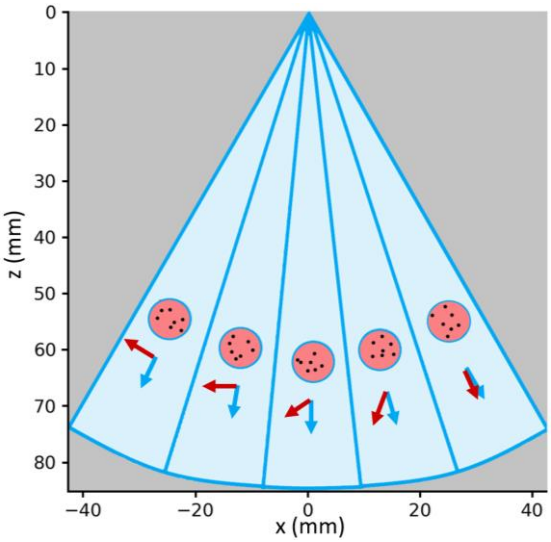

Figure 3. Cylindrical phantoms with point scatterers having different orientations (red arrows) relative to the local ultrasound beam direction (blue arrows).

Using the average amplitude inside the sector with the phantom representing fibers orthogonal to the central beam direction as a reference, we converted each other phantom's average amplitude to dB. These values were then compared to the underlying angle-to-backscatter relationship. Synthetic measurements were obtained from 10 different phantom scatterer sets for both the matrix array and 1D phased array PSFs. The mean values in dB for each probe were fit with a curve based on Equation 1, and the coefficients C_1, C_2 and C_3 were obtained. For visualization, we also simulated B-mode images of the phantoms including directionless background scatterers. For the B-mode image simulations, 700,000 isotropic background scatterers with an average intensity of -20 dB were distributed throughout the image field of view.

2.5 Simulation of Images from DT-MRI

To show the view dependence of the speckle produced by our method, we simulated images of a canine heart from a real DT-MRI volume. The volume and its geometric segmentation mask were downloaded from the Cardiovascular Research Grid[16]. Scatterers were distributed inside the volume where the segmentation mask indicated that the voxel was within the left or right ventricle. Scatterers were located pseudo-randomly inside the ventricles such that each voxel had a scatterer density of 500 per cubic mm, and orientations were set as the primary diffusion direction inside the voxel. After scatterers were distributed, 2D images were simulated from the parasternal short axis view for each probe from 0 degree and 90-degree angles. We also simulated 2D fiber images from the apical view, where the scatterers were translated across the field of view to demonstrate the changing fiber orientations relative to the beam in the apex of the heart.

2.6 Ideal Left Ventricle Phantom Simulation and Quantification

In order to measure the fiber volume processing method's performance under ideal conditions, we constructed a virtual phantom to represent a segment of a left ventricle. The segment's geometry was generated parametrically as a pair of nested truncated cones, where both the inner and outer wall were set to be exactly parallel to the local ultrasound beam direction. The segment was set to begin at z=45 mm and end at z=75 mm, and was centered at x=0 mm. The segment's inner radius was set to 12 mm at the apex and increased to 20 mm at the base, and the segment thickness increased from 6.5 mm at the apex to 11 mm at the base (Figure 4).

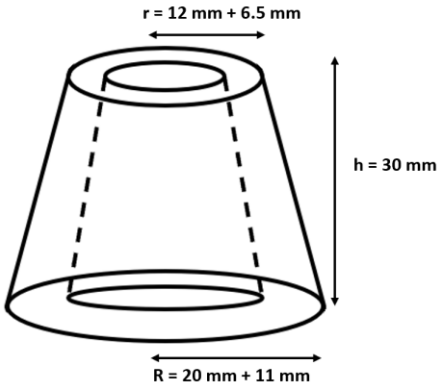

Figure 4. Geometry of a parametrically generated ideal left ventricle phantom.

A simple procedure was used to set the fiber orientation within the voxels bounded by the nested cones to mimic the orientation distributions measured throughout real human and animal left ventricles. A vector representing the circumferential direction around the z axis was rotated towards the direction of the local ultrasound beam direction based on the voxel's location within the segment, with a rotation of 0 degrees applied at the center of the segment which was linearly increased to 45 degrees at the epicardial and endocardial regions. Therefore, fiber orientations were generated to be perfectly circumferential in the midmyocardial region, with an increasing axial angle relative to both the beam direction and the ventricle surface. The axial angles in each voxel were saved as a volume, and scatterers were distributed inside the voxels as in the previous section. Ultrasound volumes were then simulated using both probes with 36 rotated planes. The volumes were processed using the previously described method and compared to the ground truth volume to obtain the average acute angle errors (AAEs).

3. RESULTS

3.1 Synthetic Rotation Phantom Imaging

Simulated b-mode images of the cylindrical fiber phantoms with isotropic, low-intensity background scatterers are shown in Figure 5. The phantoms appear brighter from right to left in both images as the orientation relative to the beam direction increases. A decrease in resolution and contrast between the phased array and matrix probes is also visible. Selected RF simulated with the matrix probe demonstrate increased signal amplitude inside the phantoms relative to the background (Figure 6), and also show that the signal increases with the fiber orientation.

The mean phantom amplitude data relative to the maximum amplitude for 10 simulated trials for each probe were fit with Equation 1, and coefficients were obtained (Figure 7). For the phased array probe, the coefficients were found to be C_1=-14.42, C_2=14.44, and C_3=-7.05. For the matrix array probe, the coefficients were C_1=-12.97, C_2=12.80, and C_3=-8.04. Our simulated measurements have close agreement with the underlying angle-to-backscatter relationship. Although the fit is better for the phased array data, a good fit is still obtained from the matrix array data.

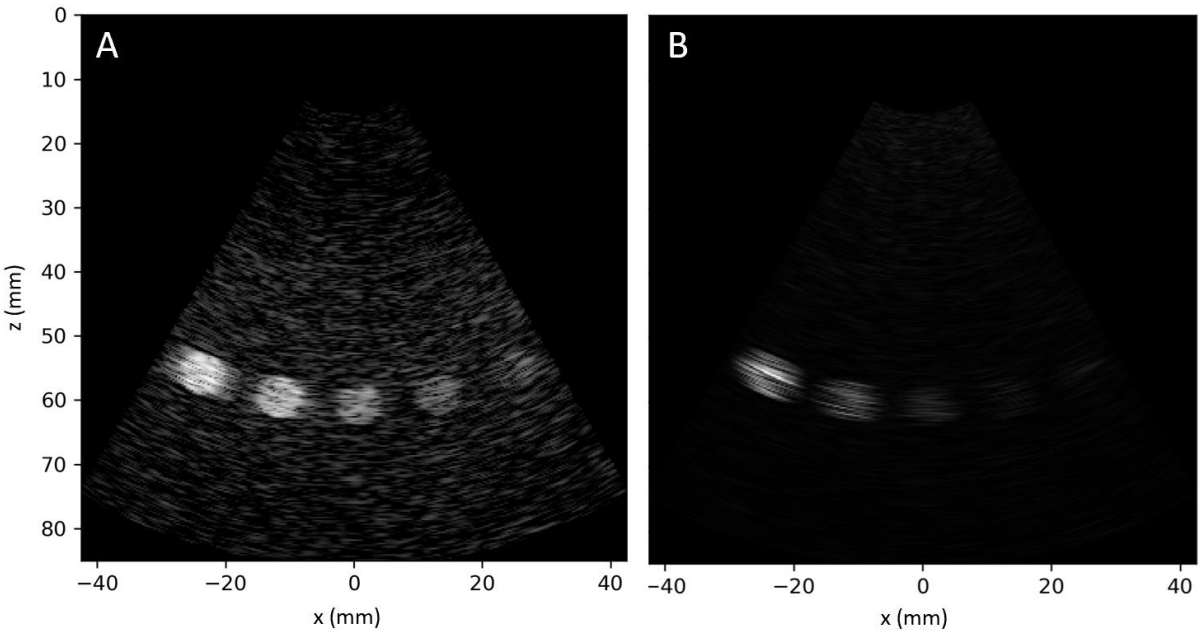

Figure 5. B-mode images of cylindrical fiber phantoms simulated with phased array probe (A) and matrix array probe (B).

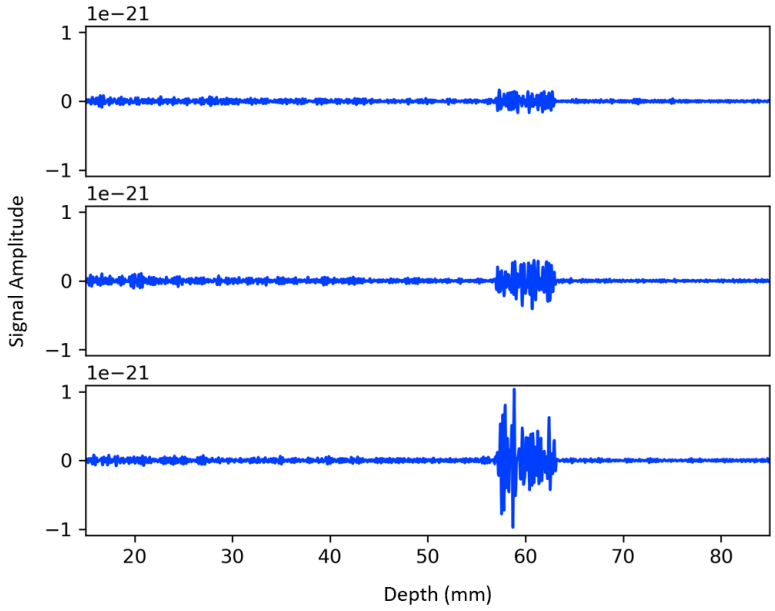

Figure 6. RF scanlines simulated with the matrix array probe. Scanlines intersect the centers of phantoms oriented at 45 degrees (top), 67.5 degrees (middle), and 90 degrees (bottom) relative to the scanline direction.

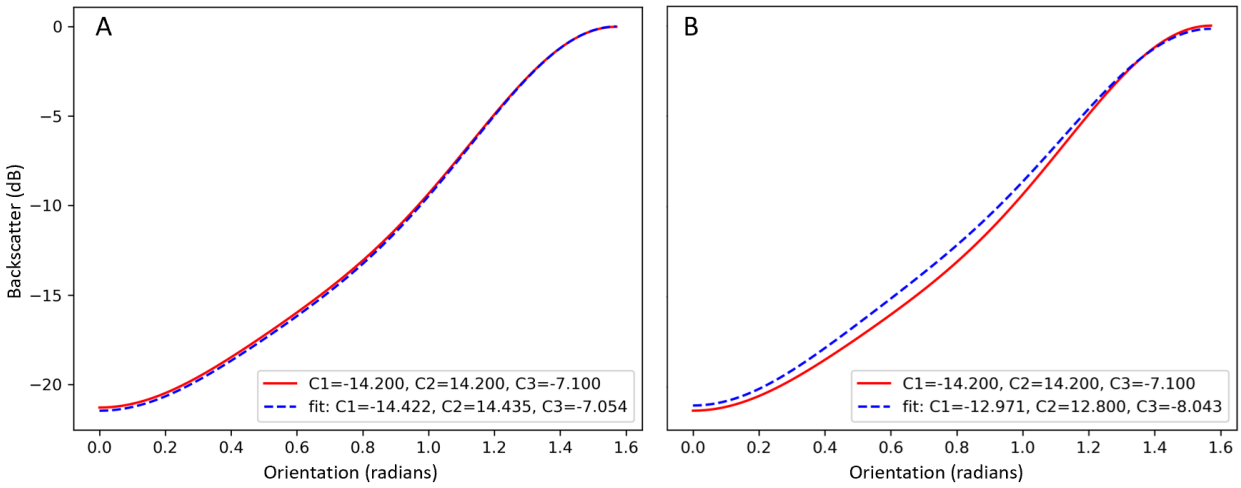

Figure 7. Angle-to-backscatter relationship obtained from data simulated with the phased array probe (A) and matrix array probe (B).

3.2 Image Simulation from Canine DT-MRI

Parasternal short axis images were simulated from DT-MRI with both probes from 0-degree and 90-degree angles (Figure 8). For our simulations, we used only the primary diffusion direction, which is known to represent the main fiber direction. The orientation according to DT-MRI is therefore visualized by taking the absolute value of the direction vector and setting the x component as the red channel, the y component as the green channel, and the z component as the blue channel (Figure 8A). The simulated images clearly exhibit view-dependent speckle, and visible details appear in both DT-MRI and simulated ultrasound images.

For the parasternal short axis view, the z component of the fiber direction vector was always perpendicular to the imaging plane as the volume was rotated around a normal vector to the plane. As can be observed in Figure 8A, few voxels have a strong z component. Therefore, most distributed scatterers were oriented such that their direction relative to the ultrasound beam changed significantly as the volume was rotated in front of the probe.

To simulate images from the apical view, we included fiber orientation processing to demonstrate that small translations of the scatterers can produce changes in the final orientation image. The heart scatterers were translated across the field of view in 12 mm increments to obtain three fiber orientation images (Figure 9). Brighter regions indicate that the fibers are oriented nearly perpendicular to the beam, and darker regions indicate orientations more parallel to the beam. The processed images exhibit noticeable differences as the volume shifts across the field of view.

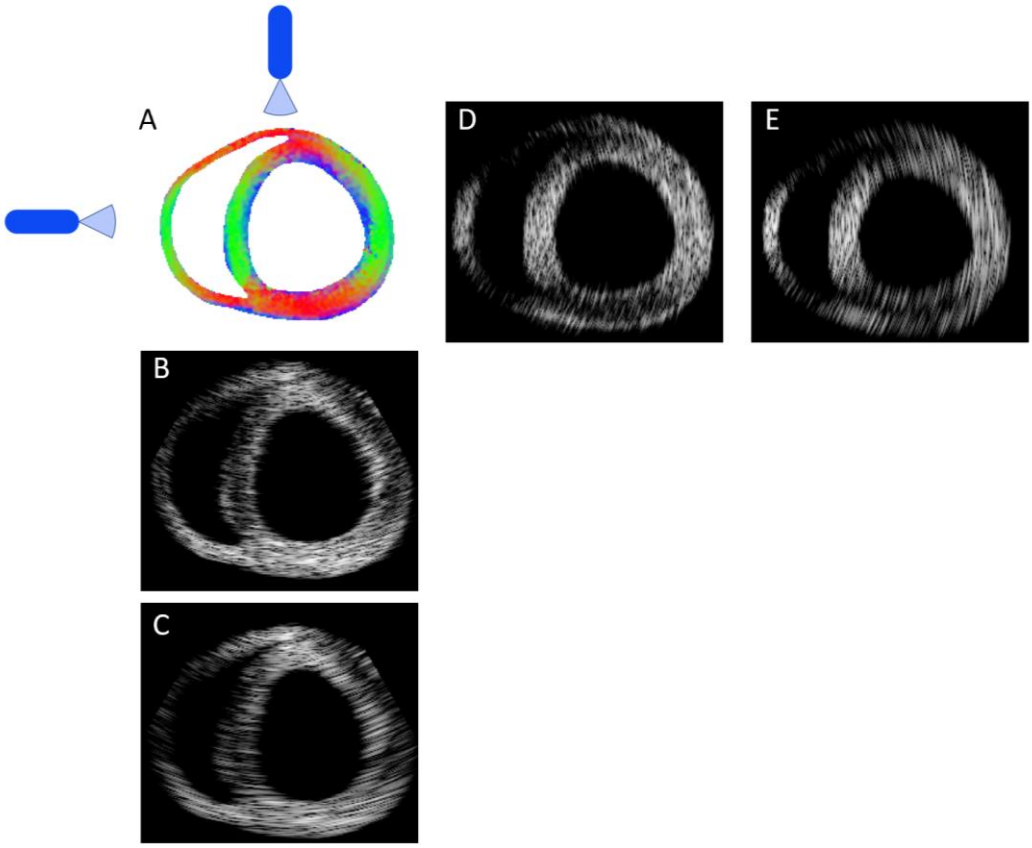

Figure 8. Parasternal short axis images of a canine heart simulated from DT-MRI slice (A) using phased array probe (B, D) and matrix array probe (C, E) at 0 degrees (B, C) and 90 degrees (D, E).

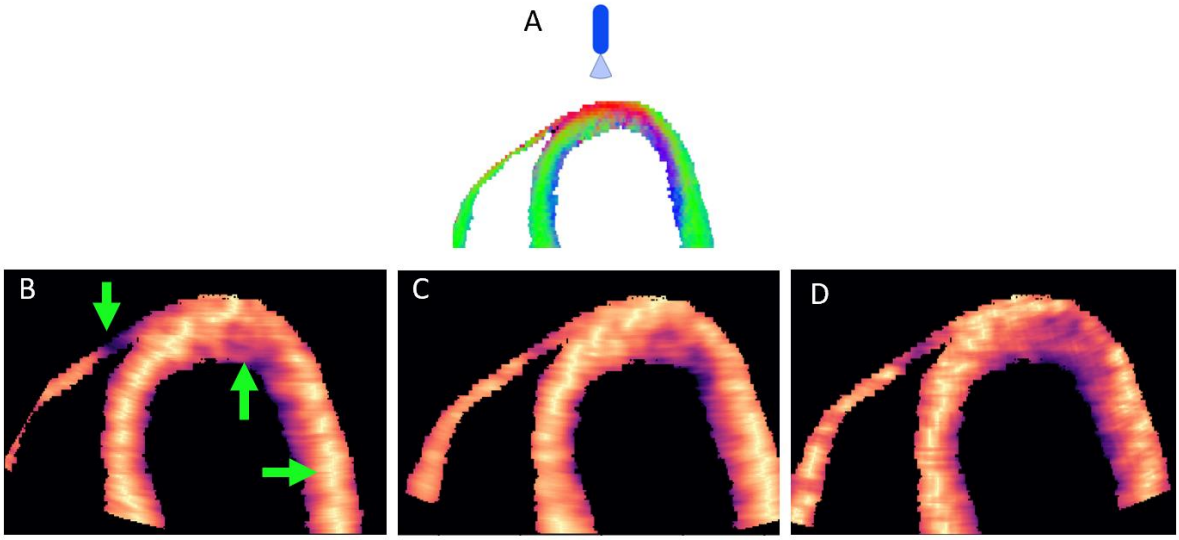

Figure 9. Fiber orientation images simulated from DT-MRI (A) from the apical view; arrows indicate regions with changes in estimated orientation as scatterers are translated in front of the transducer.

3.3 Orientation Quantification of Ideal Left Ventricle Phantom

We simulated B-mode and fiber orientation volumes from our synthetic left ventricle segment phantom using both probes (Figure 10). The fiber orientation volumes were found to have excellent agreement with the ground truth volume. The average AAE for the volume simulated with the phased array probe was 4.59 degrees, and the average AAE for the volume simulated with the matrix array probe was 7.04 degrees.

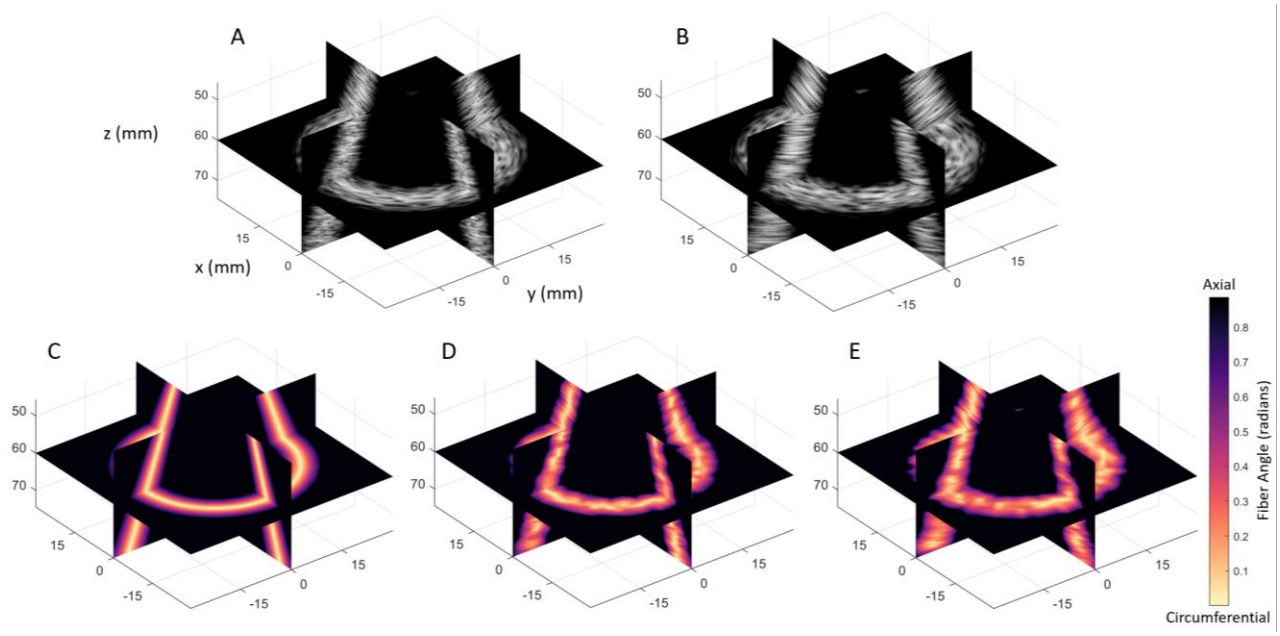

Figure 10. B-mode volumes simulated with phased array (A) and matrix array (B); ground truth fiber orientation volume (C), processed fiber orientation volumes simulated with phased array (D) and matrix array (E).

4. DISCUSSION AND CONCLUSION

Although B-mode and orientation images display a clear difference in quality between the two probes, the quantitative results for the matrix array probe are still reasonable. Our simulation results suggest that a matrix array probe transmitting diverging planar beams to image several rotated planes of interest could be used to construct cardiac fiber orientation volumes of human subjects with angle-to-backscatter based processing. Considering the ideal geometry and orientation angles of the synthetic left ventricle phantom, errors can be attributed to the relatively poor resolution of the probes and the speckle noise characteristic of ultrasound imaging. This would be further complicated *in vivo* by the complex geometry of the heart, the walls of which are unlikely to run parallel to the ultrasound beam direction in most regions. However, these limitations could be addressed using a number of methods. Deep learning-based techniques have recently achieved good results[17] for speckle reduction, and could be added to the processing pipeline to improve the image quality. Additionally, a matrix probe attached to a programmable research scanner can be configured steer an ultrasound beam in any direction. The ability to obtain backscatter intensity measurements from multiple angles could be utilized to determine fiber directions with better accuracy.

We have developed a fast, flexible method for simulating ultrasound images with view-dependent speckle and good agreement with underlying quantitative parameters. Our method can be used to validate fiber orientation quantification studies and to test approaches for image quality improvement. Furthermore, our results indicate that it is feasible to use a matrix array probe for fast analysis of fiber orientations using the angle-to-backscatter processing method.

DISCLOSURES

The authors have no relevant financial interests in this article and no potential conflicts of interest to disclose.

ACKNOWLEDGEMENTS

This research was supported in part by the U.S. National Institutes of Health (NIH) grants (R01CA156775, R01CA204254, R01HL140325, and R21CA231911) and by the Cancer Prevention and Research Institute of Texas (CPRIT) grant RP190588.

REFERENCES

[1] Tseng, Wen-Yih I., et al. "Imaging myocardial fiber disarray and intramural strain hypokinesis in hypertrophic cardiomyopathy with MRI." *Journal of Magnetic Resonance Imaging: An Official Journal of the International Society for Magnetic Resonance in Medicine* 23.1 (2006): 1-8.

[2] Papadacci, Clement, et al. "Imaging the dynamics of cardiac fiber orientation in vivo using 3D Ultrasound Backscatter Tensor Imaging." *Scientific reports* 7.1 (2017): 1-9.

[3] Dormer, James D., et al. "Estimating cardiac fiber orientations in pig hearts using registered ultrasound and MR image volumes." *Medical Imaging 2017: Ultrasonic Imaging and Tomography*. Vol. 10139. International Society for Optics and Photonics, 2017.

[4] Milne, Michelle L., et al. "Echocardiographic-based assessment of myocardial fiber structure in individual, excised hearts." *Ultrasonic imaging* 34.3 (2012): 129-141.

[5] Ramalli, Alessandro, et al. "High-Frame-Rate Tri-Plane Echocardiography With Spiral Arrays: From Simulation to Real-Time Implementation." *IEEE Transactions on Ultrasonics, Ferroelectrics, and Frequency Control* 67.1 (2019): 57-69.

[6] Jensen, Jørgen Arendt. "Simulation of advanced ultrasound systems using Field II." *2004 2nd IEEE International Symposium on Biomedical Imaging: Nano to Macro (IEEE Cat No. 04EX821)*. IEEE, 2004.

[7] Gao, Hang, et al. "A fast convolution-based methodology to simulate 2D/3D cardiac ultrasound images." *IEEE transactions on ultrasonics, ferroelectrics, and frequency control* 56.2 (2009): 404-409.

[8] Mattausch, Oliver, and Orcun Goksel. "Monte-Carlo ray-tracing for realistic interactive ultrasound simulation." *Proceedings of the Eurographics Workshop on Visual Computing for Biology and Medicine*. 2016.

[9] Alessandrini, Martino, et al. "Realistic vendor-specific synthetic ultrasound data for quality assurance of 2-d speckle tracking echocardiography: Simulation pipeline and open access database." *IEEE transactions on ultrasonics, ferroelectrics, and frequency control* 65.3 (2017): 411-422.

[10] Qin, Xulei, et al. "Simulating cardiac ultrasound image based on MR diffusion tensor imaging." *Medical physics* 42.9 (2015): 5144-5156.

[11] Hergum, Torbjørn, et al. "Fast ultrasound imaging simulation in k-space." *IEEE transactions on ultrasonics, ferroelectrics, and frequency control* 56.6 (2009): 1159-1167.

[12] Milne, Michelle L., et al. "Myocardial Fiber Mapping of Rat Hearts, Using Apparent Backscatter, with Histologic Validation." *Ultrasound in medicine & biology* 45.8 (2019): 2075-2085.

[13] Storve, Sigurd, and Hans Torp. "Fast simulation of dynamic ultrasound images using the GPU." *IEEE Transactions on Ultrasonics, Ferroelectrics, and Frequency Control* 64.10 (2017): 1465-1477.

[14] Chen, Yinran, et al. "Feasibility of multiplane-transmit beamforming for real-time volumetric cardiac imaging: A simulation study." *IEEE transactions on ultrasonics, ferroelectrics, and frequency control* 64.4 (2017): 648-659.

[15] Lam, Siu Kwan, Antoine Pitrou, and Stanley Seibert. "Numba: A llvm-based python jit compiler." *Proceedings of the Second Workshop on the LLVM Compiler Infrastructure in HPC*. 2015.

[16] Helm, Patrick A., et al. "Ex vivo 3D diffusion tensor imaging and quantification of cardiac laminar structure." *Magnetic Resonance in Medicine: An Official Journal of the International Society for Magnetic Resonance in Medicine* 54.4 (2005): 850-859.

[17] Hyun, Dongwoon, et al. "Beamforming and speckle reduction using neural networks." *IEEE transactions on ultrasonics, ferroelectrics, and frequency control* 66.5 (2019): 898-910.